General Disclaimer

One or more of the Following Statements may affect this Document

- This document has been reproduced from the best copy furnished by the organizational source. It is being released in the interest of making available as much information as possible.

- This document may contain data, which exceeds the sheet parameters. It was furnished in this condition by the organizational source and is the best copy available.

- This document may contain tone-on-tone or color graphs, charts and/or pictures, which have been reproduced in black and white.

- This document is paginated as submitted by the original source.

- Portions of this document are not fully legible due to the historical nature of some of the material. However, it is the best reproduction available from the original submission.

OLD DOMINION UNIVERSITY RESEARCH FOUNDATION

DEPARTMENT OF PHYSICS
SCHOOL OF SCIENCES AND HEALTH PROFESSIONS
OLD DOMINION UNIVERSITY
NORFOLK, VIRGINIA

Technical Report PTR-79-1

FISSION-INDUCED PLASMAS

By

W. L. Harries

and

Yuehjaw J. Shiu

Final Report
For the period December 15, 1976 - December 15, 1977

Prepared for the
National Aeronautics and Space Administration
Langley Research Center
Hampton, Virginia

Under
Research Grant NSG 1362
Frank Hohl, Technical Monitor
Environmental and Space Sciences Division

January 1979

DEPARTMENT OF PHYSICS
SCHOOL OF SCIENCES AND HEALTH PROFESSIONS
OLD DOMINION UNIVERSITY
NORFOLK, VIRGINIA

Technical Report PTR-79-1

FISSION-INDUCED PLASMAS

By

W. L. Harries

and

Yuehjaw J. Shiu

Final Report
For the period December 15, 1976 - December 15, 1978

Prepared for the
National Aeronautics and Space Administration
Langley Research Center
Hampton, Virginia 23665

Under
Research Grant NSG 1362
Frank Hohl, Technical Monitor
Environmental and Space Sciences Division

Submitted by the
Old Dominion University Research Foundation
P. O. Box 6369
Norfolk, Virginia 23508

January 1979

TABLE OF CONTENTS

LIST OF TABLES

LIST OF FIGURES

FISSION-INDUCED PLASMAS

By

W. L. Harries[1] and Yuehjaw J. Shiu[2]

1. SUMMARY

The purpose of the work was to investigate the possibility of creating a plasma from fission fragments, and to utilize the energy of the particles to create population inversion that would lead to laser action. Eventually it is hoped that the same medium can be used for both fissioning and lasing, thus avoiding inefficiences in converting from one form of energy to the other.

The work consisted of both an experimental and theoretical part. The experimental part was an investigation of various laser materials which could be used for nuclear-pumped lasing. The most likely candidate for a fissioning material in the gaseous form is uranium hexafluoride - UF_6, and experiments were performed to investigate materials that would be compatible with it. The work was done at NASA Langley in collaboration with M. D. Williams, who had constructed the apparatus, and gave very great help. The results are reported in section 2. The theoretical part can be divided into three parts, which are given in sections 3, 4, and 5.

One of the central problems in understanding a fission-induced plasma is to obtain a model of the electron behavior, and some preliminary calculations are presented in section 3. In particular, the rates of various processes are discussed. The purpose of this section is to provide a handy compendium of processes for reference. Some sections, especially 3.1.1 and 3.1.2 are largely due to J. W. Wilson of NASA Langley, but are included for convenience and because the numbers are needed later. A simple intuitive model of the electron energy

---

[1] Professor, Department of Physics, Old Dominion University, Norfolk Virginia 23508.

[2] Research Associate, Old Dominion University Research Foundation, P. O. Box 6369, Norfolk, Virginia 23508.

distribution function is also shown. The calculations are only intended to obtain orders of magnitude in many instances. The results were useful for considering a mathematical model of a nuclear-pumped laser.

Next a theoretical model of a ^{3}He-Ar nuclear-pumped laser is presented. The NASA Langley team were the first to achieve volume pumped lasing in a nuclear-pumped laser, at the Aberdeen Proving Grounds, Maryland, and hence the model could be compared with experiment. The theoretical modeling was done in collaboration with J. W. Wilson, and the results are summarized in a paper which was presented at the First International Symposium of Fission Induced Plasmas and Direct Nuclear Pumped Lasers, held at the Université Paris - Sud, Orsay, France on May 23-25, 1978. This paper, "Simplified Model of Volumetric Direct Nuclear-Pumped ^{3}He-Ar Laser," is incorporated as section 4 of this report. The theory showed good qualitative agreement with the experimental results.

A list of talks and paper connected with this grant is given in section 5.

The collaboration of NASA/Langley Research Center personnel is gratefully acknowledged, namely M. D. Williams and J. Fryer in the experimental part, section 2, and J. W. Wilson and N. W. Jalufka in section 4. We also wish to thank R. J. DeYoung of Miami University, Oxford, Ohio for his help on section 4.

2. EXPERIMENTAL INVESTIGATION OF NUCLEAR-PUMPED LASER MATERIALS

2.1. Introduction and Purpose

Hitherto nuclear-pumped lasing has been achieved using ^{3}He (volumetric pumping) and ^{10}B and ^{235}U coatings (refs. 1, 2). The ^{235}U has the largest fissioning energy (165 MeV compared to 0.76 MeV from ^{3}He) and, in the form of UF_6, has the potential of achieving a self-critical gaseous lasing system. The UF_6 molecule is not likely to lase, and the gas must be mixed with one or more materials which can absorb the fissioning energy to form inverted populations.

However, a number of difficulties could arise. Most of the nuclear-pumped lasers are recombination type, requiring a large free electron population in the plasma. The UF_6 is highly electronegative, and could attach the electrons to form negative ions, thus reducing the recombination rate and quenching the laser output. Moreover, it has many vibrational and rotational energy levels and could deexcite many excited species necessary for lasing.

In this experimental investigation, several laser systems were studied, and the effects of UF_6 were examined in order to find a laser system compatible with its presence. The experiments were carried out with electrically excited plasmas.

2.2. Experimental Arrangements

Two experimental arrangements were used (fig. 2.1). The quartz laser tubes were 80-cm long and 2.5-cm outer diameter. The ends were sealed by quartz glass windows at the Brewster angle. The electrode arrangements were of two types. In figure 2.1a the positive electrode was placed in the center of the tube, and electrodes A and B were strapped and grounded. The discharge was then along the tube axis or "longitudinal," although the fields were reversed in each half. A "transverse" discharge could be obtained by placing two brass rods along the axis (fig. 2.1b), but 100 1-KΩ resistors were soldered to rod C, with the wire connectors on their other ends facing rod D. Once a discharge occurred from one of the wires, a voltage drop occurred along the resistor which limited the discharge current, and this has the effect of more even breakdown throughout the tube. It also allowed operation at higher pressures. Voltage pulses of up to 20 kV and of 0.5-μs duration were applied to cause breakdown.

When investigating lasing, mirrors were used as shown (fig. 2.1), with the right-hand mirror either a quarter-wave dielectric, or a gold-coated hole coupled type. The light output was focused on an indium arsenide diode, which was sensitive in the 1.2-μ to 3.5-μ spectral region, and its signal displayed on an oscilloscope.

The time behavior of the light output is shown in idealized form in figure 2.2. Onset of the current usually reduced the applied voltage, which explains the "lag" between voltage and current. The laser output during the current pulse included the effects of direct electronic excitation. The pulse was usually much higher than that in the afterglow, and suffered from noise. Electronic excitation did not occur in the afterglow laser output, which showed a peak about 0.5-μs to 1-μs after the current ceased and then decayed in a few microseconds.

For spectrographic studies the front mirror was removed and the InAs diode was replaced by a variable wavelength filter or by a McPherson monochromator with a grating of 300 lines/mm. The output was not entirely independent of wavelength and showed a maximum at 3 μm because of the blazing angle of the grating. The radiation was then detected by a phototube with an S-1 spectral response (roughly 2000 to 10,000 Å) or with Polariod film, sensitive from ~2500 Å to ~6500 Å.

2.3. Results

2.3.1. CO_2.

(a) CO_2 spectra. First the spectrum of CO_2 was recorded on Polaroid film using the configuration of figure 2.1a. The spectrum appeared weak with the exception of two strong bands at 2883 Å and 2896 Å, which were probably due to the ionized molecule CO_2^+.

(b) CO_2 - UF_6. Next mixtures of CO_2 - UF_6 (up to 50 percent UF_6) were tried. The materials appeared to be chemically compatible with and without electrical pulses applied. However, spectrograms of CO_2 and CO_2 - UF_6 showed no observable difference. No lasing was detected.

(c) He - CO_2. A He-CO_2 concentration study was done with the experimental configuration of figure 2.1a, which was electrically excited at voltages of typically 20 kV. The system lased at the 1.45-μ line of the $3_p {}^1P_1 - 3_s {}^1P_1$ transition in atomic carbon. A very small amount of CO_2 was needed to obtain lasing at 100-torr total pressure. Variation of laser output versus CO_2 partial pressure (fig. 2.3) shows that the maximum output occurred for a CO_2 concentration of 0.04 percent.

(d) He-CO_2-UF_6. The experiment on He-CO_2-UF_6 mixtures was done with the configuration of figure 2.1b with typical peak voltages of 10 kV. Lasing at the 1.45-μ carbon line could not be obtained in either He-CO_2 or He-CO_2-UF_6 (up to 10 percent) mixtures. The causes for not lasing were not definitely known; however, the difference in electrode configuration and/or possible UF_6 contamination on the walls inside the tube may have been the reasons.

2.3.2. N_2. - The N_2-UF_6 spectrographic study was done in both the configurations of figure 2.1. Type (b) was used to achieve higher gas pressures.

(a) N_2 spectra. At 5 torr and 150 torr, N_2 band spectra appeared very strongly at the second positive transition ($C^3\pi - B^3\pi$). Relative intensities are given in figure 2.4. The most prominent transitions were the 3371.3 Å (0,0) and 3576.9 Å (0,1). Some of the N_2 first negative system and CN spectra were also observed.

(b) N_2-UF_6. A total pressure of 50 torr and UF_6 concentrations from 1 to 10 percent were used in the N_2-UF_6 mixture. There were no obvious changes in the emission spectra, with the exception of a Si line which appeared at 2881.58 Å with the addition of UF_6. No laser action was found at 3371 Å or 3576 Å, possibly because of the slow rise time (150 ns) of the electrical excitation (ref. 3).

2.3.3. Cl_2.

(a) He-Cl_2. A mixture of He-Cl_2 was found to lase at the 1.587-μm Cl line (3d ^{4}F9/2-4p ^{4}D7/2) (ref. 4). The effect of the percentage of Cl_2 on the laser output at a total pressure of 200 torr is given in figure 2.5a. The maximum laser output occurred at 0.2 percent Cl_2; lasing occurred only during the afterglow.

(b) He-Cl_2-UF_6. Adding UF_6 at a total pressure of 200 torr quenched the laser output very rapidly. The laser output at 1.587 μm was decreased by 90 percent with 3 percent UF_6, and laser action terminated at $\lesssim$4 percent UF_6 (fig. 2.5b).

2.3.4. Ar.

(a) He-Ar. The He-Ar (1% Ar, total pressure 100 torr) system (ref. 4) lased at the 1.79-μm, 2.9-μm, 2.2-μm, and 1.2-μm Ar lines. The 1.79-μm line ($3d[1/2]^\circ_1$ - $4p[3/2]_2$) was the strongest. Laser signals were observed during both the current pulse and afterglow period.

(b) He-Ar-UF_6. The 1.79-μm Ar line was studied with varying amounts of UF_6 added to the He-Ar mixture (fig. 2.6). Curve (a) is the direct electron excitation output, and curve (b) is for the afterglow. At $\lesssim$2 percent UF_6, lasing in the afterglow stopped, while direct electron excitation lasing (initial laser pulse) decreased gradually, and completely ceased at $\lesssim$8 percent UF_6.

2.3.5. Xe.

(a) He-Xe. This system (2% Xe, total pressure 60 torr) (refs. 4,5) was found to lase at the Xe lines, 3.5-μm ($5d[7/2]^\circ_3$ - $6p[5/2]_2$), 2.02-μm ($5d[3/2]^\circ_1$ - $6p[3/2]_1$), 2.65-μm ($5d[3/2]^\circ_1$ - $6p[1/2]_0$), and 3.65-μm ($7p[1/2]$ - $7s[3/2]^\circ_2$). The 3.5-μm line was the strongest.

(b) He-Xe-UF_6. The effect of adding UF_6 to the He-Xe mixture lasing at the above-mentioned laser lines is shown in figure 2.7, which shows lines from the first pulse which were excited by direct electron impact excitation. In many cases severe arcing occurred due to the large amount of UF_6 in the laser tube, and high percentages of UF_6 were very difficult to work with. However, laser action was observed even up to 20 percent UF_6 at 60 torr of total pressure. The afterglow lines are not shown in figure 2.7, and suffered the greatest attenuation. The 2.65-μm Xe line (which lased only in the afterglow) was attenuated most, and was completely quenched at < 5 percent UF_6. The 2.02-μm and 3.5-μm lines were completely attenuated at 7 percent UF_6. At a fixed percentage of UF_6 (10%) the laser output vs. percentage of Xe was measured with gold-coated hole coupled mirrors and found to maximize at ≈ 4 percent Xe (fig. 2.8).

(c) Ar-Xe. The Ar-Xe system (200-torr total pressure) (ref. 6) lased at the xenon lines 2.65 μm ($5d[3/2]_1^\circ$ - $6p[1/2]_0$), 2.62 μm ($5d[5/2]_2^\circ$ - $6p[5/2]_2$), 2.02 μm ($5d[3/2]_1^\circ$) - $6p[3/2]_1$) and 1.73 μm ($5d[3/2]_1^\circ$ - $6p[5/2]_2$). Of these the 2.65-μm line, which lased both during the current pulse and afterglow, was the strongest. It was observed that all these laser lines were from the 5d level of excited Xe. A concentration study (fig. 2.9) showed that the afterglow laser output had a maximum at about ≈ 4 percent Xe for the 2.65-μm line.

2.3.6. Kr.

(a) He-Kr (ref. 7). A He-Xr mixture (0.1% Kr, 600-torr total pressure) lased at the following Kr lines: 1.784 μm ($4d[1/2]_0^0$ - $5p[1/2]_1$), 2.524 μm ($4d[1/2]_1^\circ$ - $5p[3/2]_2$) and 3.0672 μm ($6p[1.2]_1$ - $6s[3/2]_2^\circ$). The 1.784-μm line was the strongest. A comparison of the output for the 1.78-μm Kr line (He-Ar mixture) with the 1.79-μm Ar line

(He-Ar mixture) was made. The total pressure was 600 torr in each case, and the concentrations were those for optimum power, namely 0.12 percent Kr and 0.6 percent argon respectively. Voltage pulses of about 3 kV lasting for 0.5 μs were applied using the arrangement in figure 2.1b. The time behavior of the laser pulses was similar, with a steep rise to a peak in about 1 μs, followed by a decay. The peak power of the He-Kr laser was about 1.4 times that of the He-Ar, and the signals dropped to 1/3 peak value in approximately 1.5 μs(Kr) and 0.7 μs(Ar), with total durations of 2.5 and 1.5 μs respectively.

(b) He-Kr-UF_6. With 0.12 percent UF_6 added to the He-Kr mixture (0.12% Kr, 600-torr total pressure), the 1.78-μm Kr laser line, which previously decayed with time in the afterglow, was now observed to have a maximum about 1 μs after the voltage became zero. The laser duration also increased from 2.5 μs to 4.5 μs. However, higher percentages of UF_6 caused severe arcing, and no definite conclusion can be drawn at present.

2.4. Discussion and Conclusions

The major purpose of this experimental investigation was to find a laser system compatible with UF_6 for nuclear pumping. So far, most of the laser systems under investigation were recombination types: He-Cl_2, He-Ar, He-Xe, etc. It appeared that adding UF_6 to these laser systems resulted in a decrease or quenching of the laser output, suggesting that recombination type lasers might not be suitable for nuclear pumping. However, among the systems studied, the 3.5-μm Xe line (He-Xe mixture) exhibited high gain when the excitation process involved direct electron excitation from the ground state. Also, the He-Xe-UF_6 system was observed to lase at $\geq$10 percent UF_6 with a relatively high percentage of Xe ($\geq$4%) for maximum laser output. This system might also be promising for nuclear pumping. A mixture of He with 10 percent UF_6 and 5 percent Xe at a total pressure of 600 torr is probably the optimum combination for testing at the reactor site.

Not all the above systems however, need necessarily have acted as recombination type lasers, and it is possible that a different pumping mechanism could have occurred in the Ar-Xe mixture, which yielded the 2.65-μm Xe line. In the He-Xe system both 7p→7s and 5d-6p transitions were observed, whereas in the Ar-Xe system only the 5d-6p transitions occurred. The difference in species formation implies pumping of the upper laser level through the formation of Ar_2^*, which subsequently transferred its energy to the 5d levels of Xe. If so, the pumping would not require electrons for recombination, and should work well with UF_6. Further studies on He-Xe and Ar-Xe should be carried out to provide a basic understanding of the pumping process in these two systems.

A ^{3}He-Kr nuclear laser pumped by neutrons from a reactor has been found to lase at the 2.52-μm Kr line (refs. 4,7), but its power output was very low compared to ^{3}He-Ar at the 1.79-μm Ar line (ref. 4). In contrast here with electrical excitation it was found that the 1.78-μm Kr line was the strongest of the Kr lines, with the lasing power ratio of $\frac{p(Kr)}{p(Ar)} \approx 0.7$ at their peak laser outputs and optimum concentration. Also, the 1.78-μm Kr line had a longer pulse than the 1.79-μm Ar line, so that their total energy output was comparable. Our result suggests that the 1.78-μm Kr line should be further studied with nuclear pumping both by cylindrical and box lasers. There should be no optical alignment difficulties because the 1.79-μm Ar line and 1.784-μm Kr line are so close, although mirror adjustments seem more sensitive for Kr line than Ar line.

2.5. References

1. DeYoung, R. J.; Jalufka, N. W.; Hohl, F.; and Williams, M. D.: Proceedings of the Princeton Conference on Partially Ionized Plasmas. Third Symposium on Ur Plasmas (Princeton, NJ), pp. 96-101, June 10-12, 1976.

2. Prelas, M. A.; Akerman, M. A.; Boody, F. P.; and Miley, G. H.: Appl. Phys. Lett., Vol. 31, p. 428, 1977.

3. Akins, R. P.; and Lin, S. C.: Appl. Phys. Lett., Vol. 28, p. 221, 1976.

4. DeYoung, R. J.; Jalufka, N. W.; and Hohl, F.: AIAA, Vol. 16, p. 991, 1978.

5. Mansfield, C. R.; Bird, P. R.; Davis, J. F.; Wimett, T. F.; and Helmick, H. H.: Appl. Phys. Lett., Vol. 30, p. 640, 1977.

6. Newman, L. A.; and DeTemple, T. A.: Appl. Phys. Lett., Vol. 27, p. 677, 1975.

7. DeYoung, R. J.; Jalufka, J. W.; and Hohl, F.: Appl. Phys. Lett., Vol. 30, p. 19, 1977.

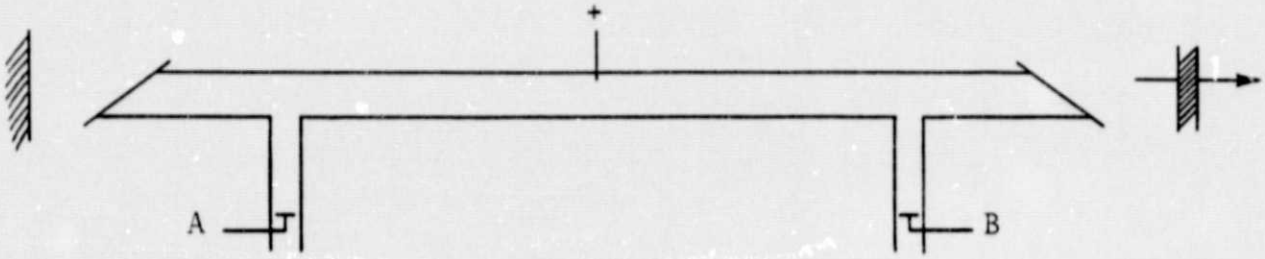

(a) Longitudinal discharge. Electrodes A and B are connected and grounded.

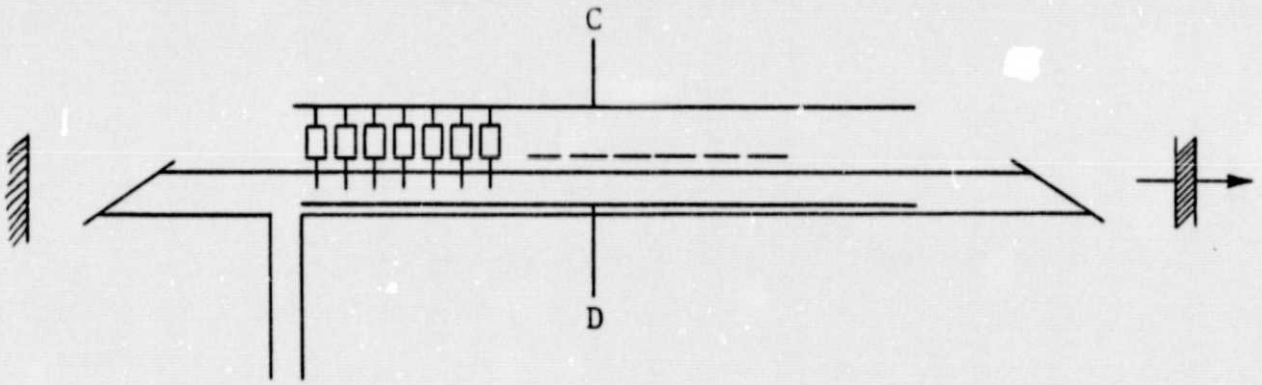

(b) Transverse discharge. Electrode C consisted of 100 wires connected to 1-K resistors, to cause even breakdown throughout the vessel.

Figure 2.1. Experimental arrangements.

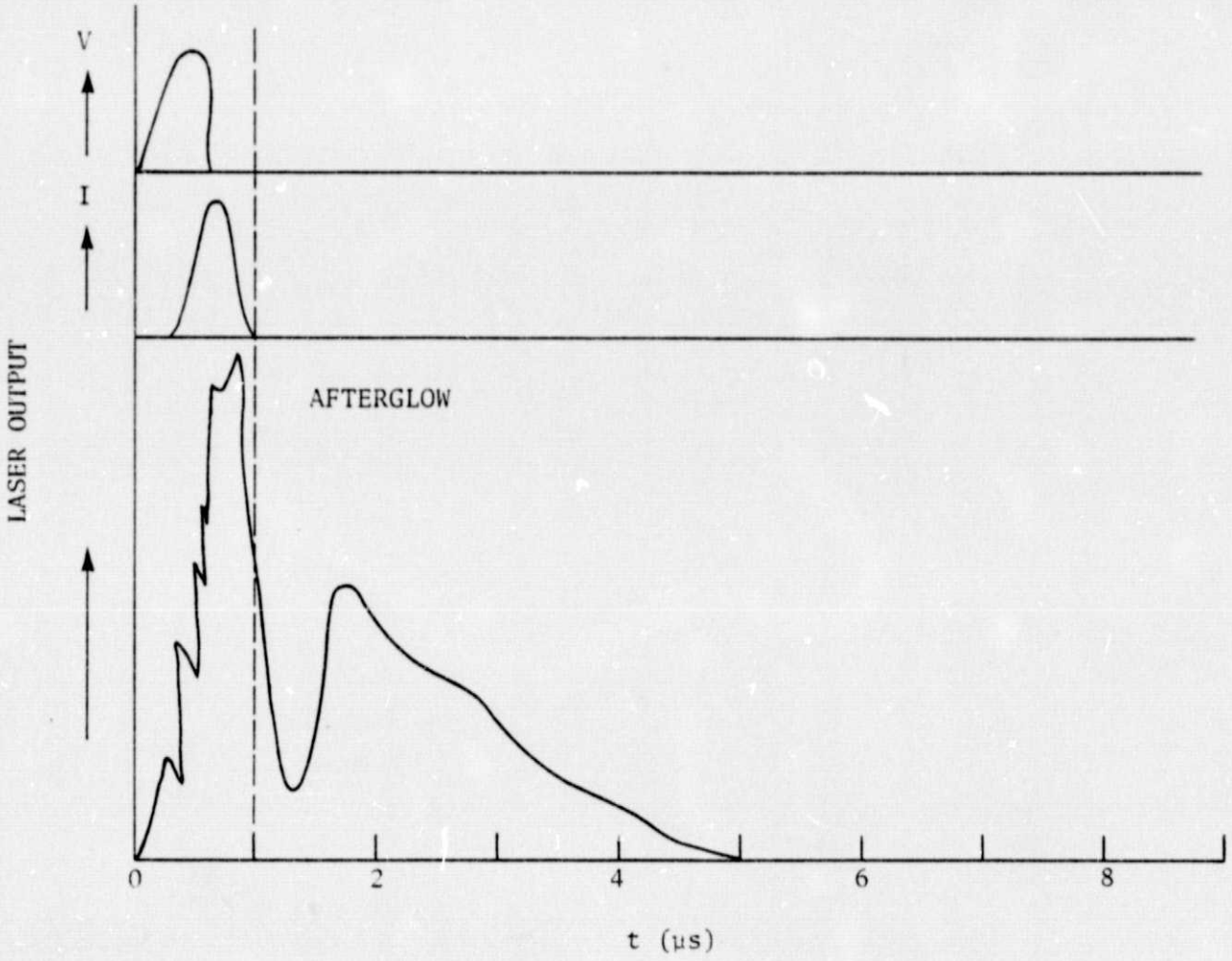

Figure 2.2. Idealized time behavior of laser pulses. The leading edge of the light signal was subject to noise pickup.

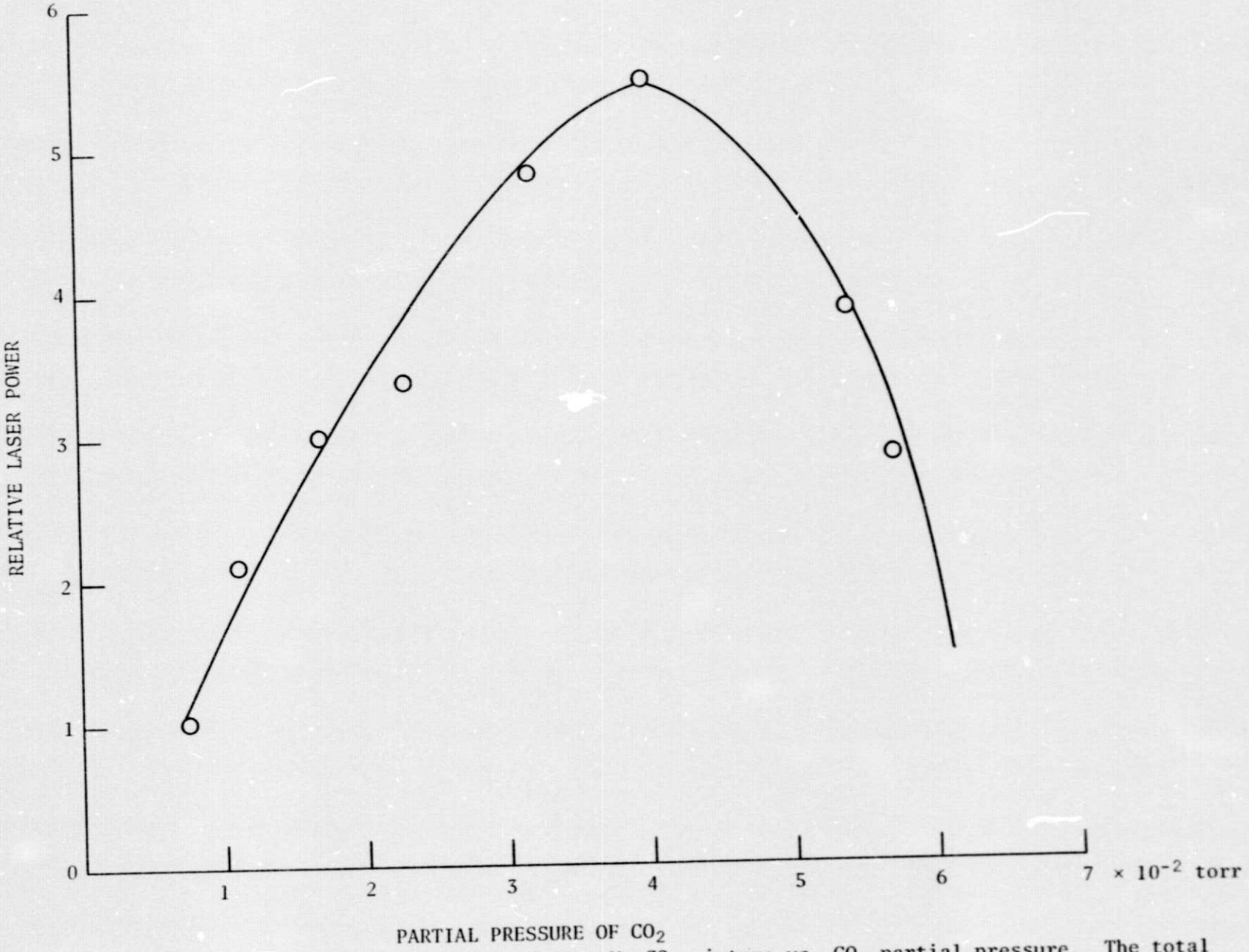

Figure 2.3. Relative laser output power from a He-CO_2 mixture vs. CO_2 partial pressure. The total pressure was 100 torr.

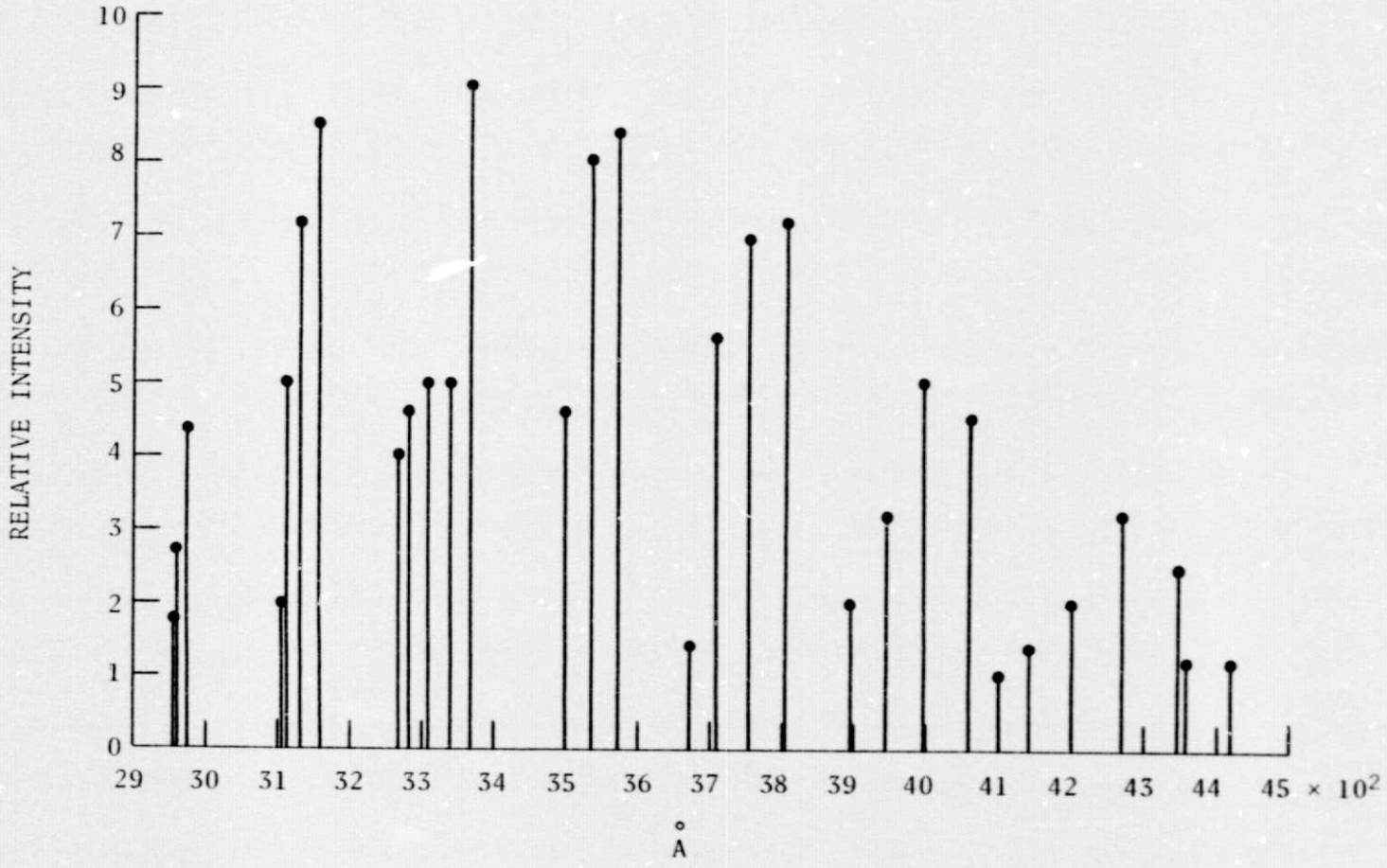

Figure 2.4. N_2 second positive spectrum. The relative density was not corrected by the quantum efficiency of the phototube.

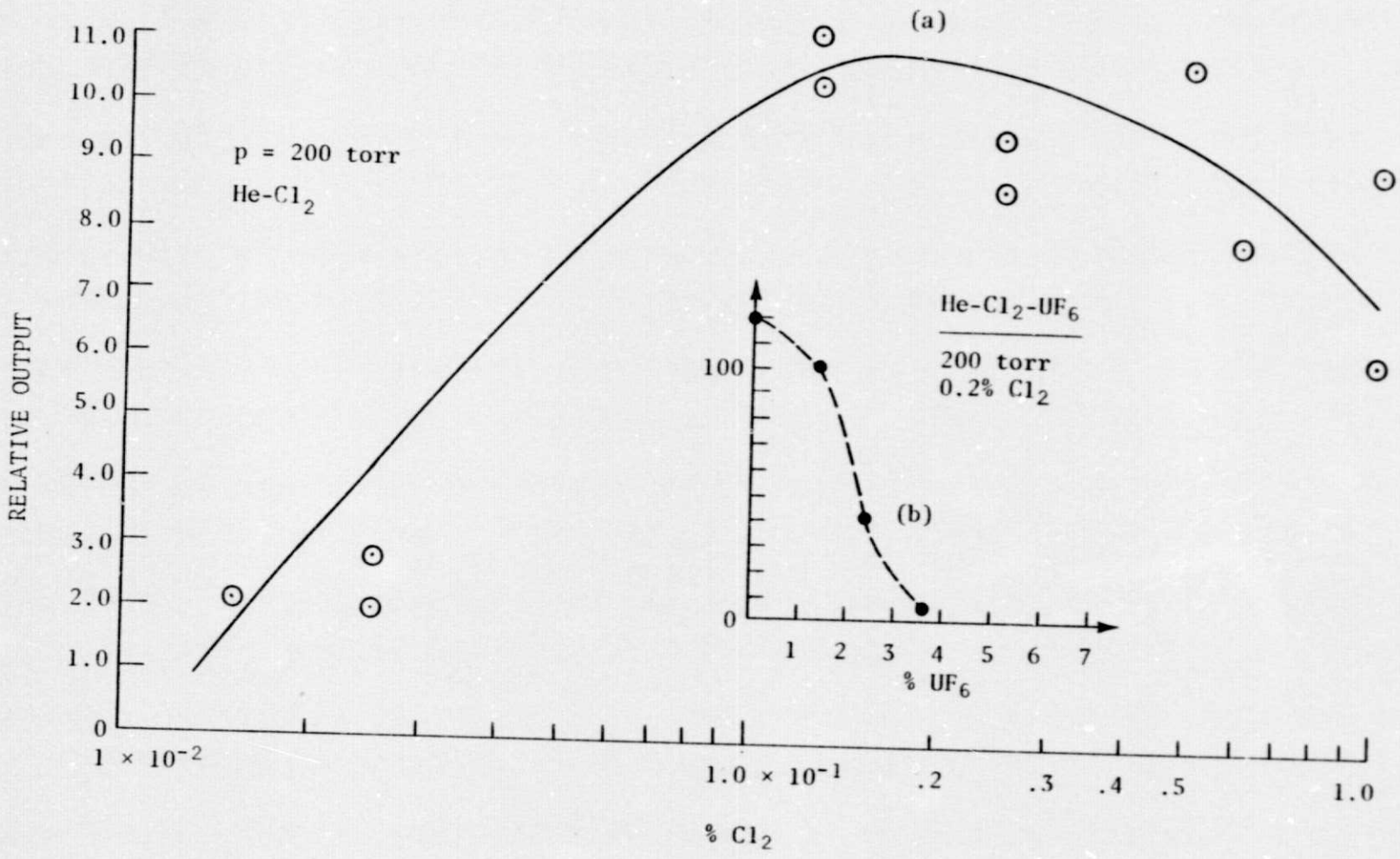

Figure 2.5. (a) Relative laser output of the 1.587 μm Cl line vs. % Cl_2 in a He-Cl_2 mixture. (b) Relative output from He-Cl_2-UF_6 vs. % UF_6.

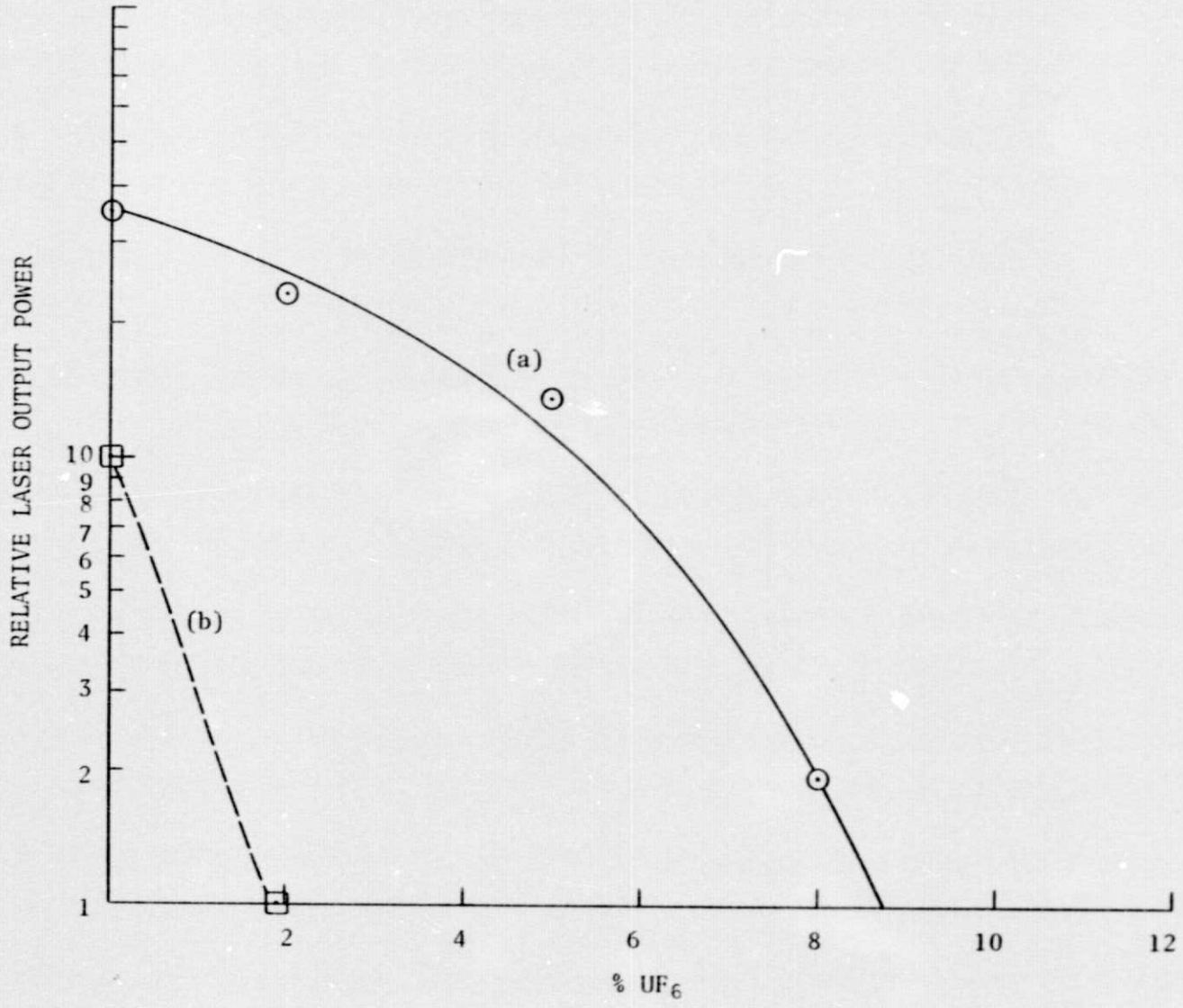

Figure 2.6. Relative laser output power from a He-Ar-UF_6 mixture vs. UF_6 concentration. Total pressure of 100 torr: (a) direct electron excitation lasing, (b) afterglow laser output.

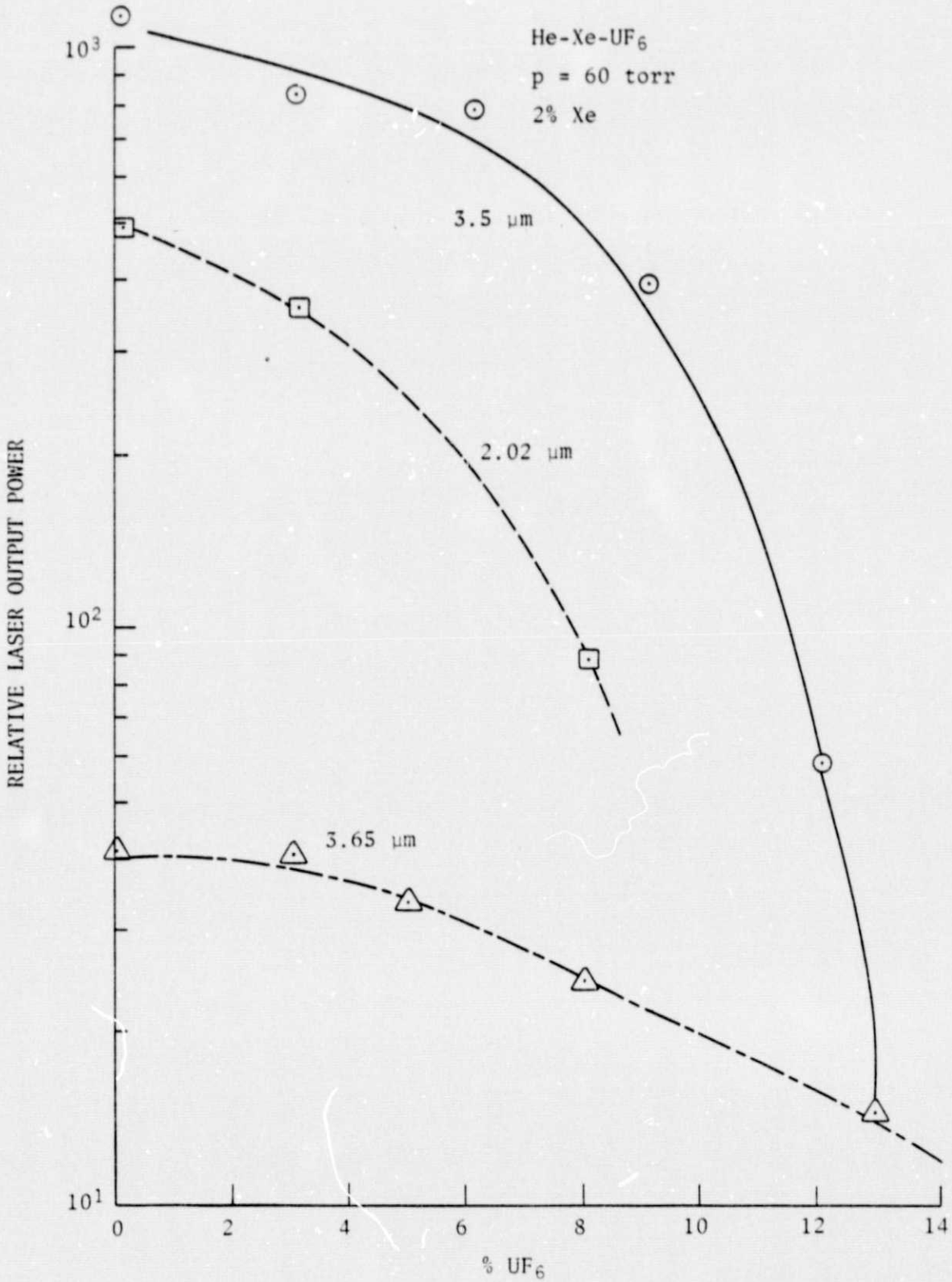

Figure 2.7. Relative laser output power of the initial laser pulse from a He-Xe-UF_6 mixture vs. UF_6 concentration.

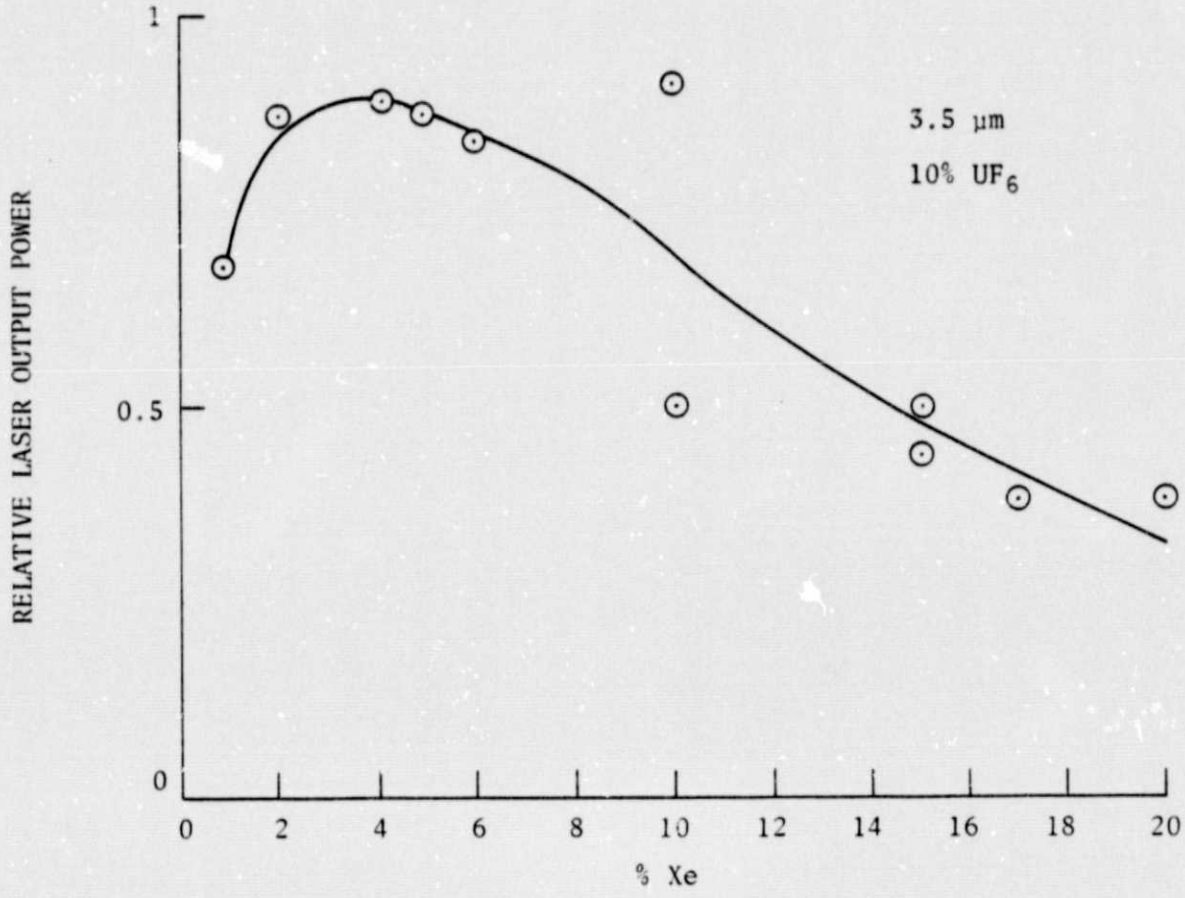

Figure 2.8. Relative laser output power from a He-Xe-UF_6 mixture vs. Xe concentration.

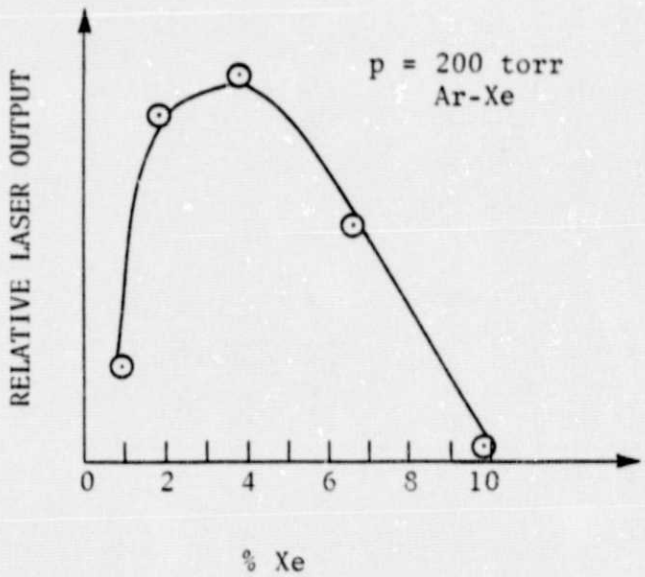

Figure 2.9. Relative laser output power from an Ar-Xe mixture vs. Xe concentration (2.65-μm Xe line).

3. PRELIMINARY CALCULATIONS ON ELECTRON BEHAVIOR IN A FISSION-INDUCED PLASMA

3.1. Introduction

The purpose of this section is to obtain a model for the electron behavior in a fission-induced plasma and to see which processes dominate. In particular, approximate values are obtained for the rates of various processes such as recombination, energy loss, ionization, excitation, energy transfer, and particle losses. An intuitive treatment of the electron energy distribution is also included. We consider the electrons to be in a background of ^3He, but the results will also apply for small admixtures of other gases.

3.2. Production of Electrons

The electrons are produced by the products of the action of thermal neutrons on He^3:

$$n + He^3 \rightarrow p(0.57\ MeV) + T(0.19\ MeV)$$

Both proton and triton ionize. On the average, 34 eV are needed to produce one electron-ion pair, and the electron receives an average of 8-eV kinetic energy; thus, 20 percent goes in kinetic energy (ref. 1). Hence, the number of electrons produced per neutron, Q, is

$$Q = [(0.57 + 0.19)MeV/(34 + 8)eV] \approx 2 \times 10^4 \text{ electrons}$$

If the fast-burst reactor produces a flux, F, of 10^{17} neutrons/cm^2/s, and they are absorbed with an average range r = 6 cm, then the number of electrons produced per second per cubic centimeter is

$$\left(\frac{dN}{dt}\right)_{prod} \approx QFr^{-1} = 3 \times 10^{20}\ el/cm^3 \cdot s$$

A more accurate estimate is based on a calculation by Wilson (ref. 1) for the energy deposited/neutron cm^2, in unit volume, which is 0.3 $MeV/cm^3 \cdot$ neutron$\cdot cm^2$ for p = 3 atmospheres. Multiplying this by the flux gives the energy input per cubic centimeter per second, namely, 3×10^{22} $eV/cm^3 \cdot s$. Assume that at one atmosphere the energy deposited is one-third as much, or 10^{22} $eV/cm^3 \cdot s$. The production rate of electrons is thus 10^{22} $(eV\ cm^{-3} s^{-1})$ (34 + 8) $eV \approx 2 \times 10^{20}$ el/cm^3

assume

$$\left(\frac{dN}{dt}\right)_{prod} \approx 2 \times 10^{20}\ el/cm^3 \cdot s$$

3.3. Loss Mechanisms and Plasma Containment Time

Experimentally, the pulses are $\approx$ 1/2-ms long, but the electron containment time, τ_c could be much shorter. Rough estimates of τ_c can be made by (1) assuming the electrons diffuse out of the plasma to the walls, or (2) by assuming that recombination dominates the lift time.

3.3.1. Containment time by diffusion to the walls. - The containment time, τ_c, assuming diffusion of electrons to the wall, is given by

$$\tau_c \approx \frac{x^2}{D_a}$$

where x is a characteristic distance $\approx$ 1 cm, and D_a the ambipolar diffusion coefficient. The diffusion coefficient for helium has been measured (ref. 2) as $D_a = 700 \pm 50$ $cm^2\ s^{-1}$ at 1 torr, so $\tau_c \approx 1$ s at 760 torr, much longer than the observed pulse length. Hence, diffusion is not important.

3.3.2. Containment time by recombination. - The recombination rate depends on whether He^+ or He_2^+ dominates. For the former, three recombination processes can occur, namely (1) radiative, (2) collisional radiative ($He^+ + e + e \rightarrow He^* + e$), or (3) neutral stabilized ($He^+ + e + He \rightarrow He^* + He$). Processes (2) and (3) are orders of magnitude faster than (1). However, with the type of discharges here it seems He_2^+ should dominate. In addition to processes

analogous to (2) and (3), dissociative recombination ($He_2^+ + e \rightarrow He^* + He$) is also possible. The recombination rates of He^+ from (2) and (3), and the recombination of He_2^+, turn out to be the same order of magnitude, which yields $(dn/dt)_{ioss}$ for electrons in terms of n, the electron density.

3.3.3. Steady-state density of electrons. - Assuming steady state, and equating the production and loss rates, yield

$$n \approx 10^{13}/cm^3$$

and the containment time, τ_c, defined by

$$\left(\frac{dn}{dt}\right)_{loss} = \frac{n}{\tau_c}$$

is of order 10^{-7} s, and much less than the pulse duration of 5×10^{-4} s. The values of n and τ are roughly the same irrespective of whether He^+ or He_2^+ dominates.

3.4. Electron Energy Loss Rates

The electrons are created at energies up to several keV, and thereafter they lose their energy by inelastic and elastic collisions.

3.4.1. Energy losses by inelastic collisions. - In the range $20 < \varepsilon < 2000$ eV, the most rapid energy loss rate for electrons is due to inelastic collisions of ionization and excitation of both neutrals and ions. The rate of change of the energy ε of one electron with time is

$$\frac{d\varepsilon}{dt} = -\nu_1 E_1 - \nu_2 E_2 - \ldots = -\overline{\nu E} \qquad (1)$$

where ν_n is the collision frequency for level n, and E_n is the energy given up by the electron. The quantity $\overline{\nu E}$ is an average for all levels,

where

$$\nu = \frac{v_r}{\lambda} = N\,\overline{\sigma v_r} \tag{2}$$

and v_r is the electron random velocity, λ is the mean free path, N is the density of targets, and σ the cross section for inelastic collisions. Here we are concerned with orders of magnitude only and assume λ = constant. Then

$$v_r = (2\varepsilon/m)^{1/2} \tag{3}$$

and

$$\frac{d\varepsilon}{dt} = N\sigma \left(\frac{2\varepsilon}{m}\right)^{1/2} E = \left(\frac{2}{m}\right)^{1/2} \frac{E}{\lambda}\, \varepsilon^{1/2} \tag{4}$$

Thus the energy of the electrons varies with time according to

$$\varepsilon = \varepsilon_o \left(1 - \left[\frac{E}{\sqrt{2m\varepsilon_o}\ \lambda}\right] t\right)^2 = \varepsilon_o \left(1 - \frac{t}{T_{in}}\right)^2 \tag{5}$$

where ε_o is the initial energy of the electron and T_{in} is a characteristic time for inelastic energy loss,

$$T_{in} = \left[\frac{\varepsilon_o^{1/2}\ \lambda\ \sqrt{2m}}{E}\right] \tag{6}$$

The excitation cross section for He above 19 eV is 0.5×10^{-7} cm^2 (ref. 2), and the number of atoms/cm^3 at 760 torr is 2.5×10^{19}. Hence $\lambda = (N\sigma)^{-1} = 7.4 \times 10^{-5}$ m. The value of T_{in} depends on the choice of ε_o, and if $\varepsilon_o \approx 1$ keV, and E $\approx$ 20 eV, then $T_{in} \approx 4 \times 10^{-10}$ s.

In the energy regime from 2 keV down to a few volts, elastic collisions will contribute little to energy loss (see the following pages).

3.4.2. Energy losses below 20 eV. - Equation (5) will describe the energy versus time down to a few eV. The last inelastic collision will take place at the first excited state of He, which is 19.6 eV. The impacting electron will have an energy somewhat over 20 eV, and will possess $\approx$ 1 eV after the collision. At 19.6 eV the inelastic cross section becomes zero, and below this energy the electrons can only lose energy by elastic collisions. The elastic collisions will be of two kinds--against neutrals (assumed at around room temperature) and against other electrons or ions, where long-range Coulomb-type collisions take place.

3.4.3. Elastic collisions with neutrals. - The rate of change of electron energy versus time for one electron from collisions with neutrals is

$$\frac{d\varepsilon}{dt} = -\kappa\, \varepsilon\, \nu_e \tag{7}$$

where κ is the average fraction of its energy lost in the collision, and

$$\kappa = 2m/M = 1/3000$$

for electrons in ^{3}He. The collision frequency ν_e here is the elastic collision frequency and is equal to v_r/λ_e. From equations (7) and (3) an energy versus time relation is obtained when elastic collisions with neutrals dominate,

$$\frac{d\varepsilon}{dt} = -\frac{\kappa}{\lambda}\sqrt{\frac{2}{m}}\,\varepsilon^{3/2} \tag{8}$$

and if the electron starts with an energy ε_1 then

$$\varepsilon = \varepsilon_1\left[1 + \left(\frac{\kappa}{\lambda_e}\sqrt{\frac{2}{m}}\,\varepsilon_1^{1/2}\right)t\right]^{-2} = \varepsilon_1\left[1 + \frac{t}{T_{e,n}}\right]^{-2}\ , \tag{9}$$

Here $T_{e,n}$ is a characteristic time to reduce the energy to $\varepsilon_1/4$:

$$T_{e,n} = \frac{\lambda_e}{\kappa}\sqrt{\frac{m}{2}}\,\varepsilon_1^{-1/2} \tag{10}$$

Assuming $\varepsilon_1 \approx 1$ eV and λ_e, the mean free path for electron-neutral collisions in He^3 at 1 torr is 17.6×10^{-3} (ref. 4), then $\lambda_e = 2.3 \times 10^{-7}$ m at one atmosphere, and

$$T_{e,n} \approx 10^{-9} \text{ s}$$

for the range 1 to 1/4 eV. The function $\varepsilon(t)$ approaches $\varepsilon = 0$ asymptotically. The time required to reduce ε from $\varepsilon_1 = 1$ eV down to 1/40 eV is 24 ns. Note $T_{e,n} \propto v_r^{-1}$, and the range of ε_1 must be taken into account.

3.4.4. Elastic collisions with cold electrons. - A measure of the rate of energy loss of electrons of temperature T to electrons of temperature T_1 can be obtained from the equipartition time τ_{e-e}. Strictly speaking this time is a measure of the rate at which equipartition of energy is established between two groups of particles, namely test particles in a Maxwellian distribution and at a temperature T, and field particles at a temperature T_1. The collisions are assumed to be long-range Coulomb collisions. The equipartition time τ_{eq} is defined by the equation (ref. 5)

$$\frac{dT}{dt} = - \frac{T - T_1}{\tau_{eq}} \tag{11}$$

and

$$\tau_{eq} = \frac{3.3 \times 10^5 \ \varepsilon^{3/2}}{n \ln \Lambda} \text{ (s)}; \ T_1 \to 0 \tag{12}$$

with $\varepsilon = T$ (eV), electron density n in cm^{-3}, and Λ is the ratio of the Debye length to the impact parameter. Assume here that $T_1 = 1/40$ eV, $<< T$, and let T be 10 eV and 1 eV respectively. The values of $\ln \Lambda$ change little with n and T, and the values for τ_{eq} are shown in the following table.

		Values of τ_{eq} in s for	
Ne cm^{-3}	ln Λ	T = 1 eV	T = 10 eV
10^{11}	10.7	3.0×10^{-7}	10^{-5}
10^{12}	9.6	3.4×10^{-8}	10^{-6}
10^{13}	8.5	3.8×10^{-9}	10^{-7}
10^{14}	7.3	4.4×10^{-10}	1.4×10^{-8}

For $n = 10^{13}/cm^3$, $T_1 = 1$ eV, the time for the hot electrons to be cooled by electrons at room temperature is of order $T_{e,n}$. For energies less than 1 eV the electron-electron collisions dominate as $\tau_{eq} \propto v_r^3$.

3.4.5. Elastic collisions with ions. - The ions, being of equal mass with the neutrals, should be quickly cooled, and should then cool the electrons. However, the equipartition time for the electrons to be cooled by ions at room temperature, namely $\tau_{eq,e-i}$, is far greater than the electron-electron cooling time $\tau_{eq,e-e}$ (ref. 5):

$$\tau_{eq,e-e}/\tau_{eq,e-i} = m/M_i = 1/6000 \tag{13}$$

where M_i is the mass of the ion, and the cooling of electrons by ions can be neglected.

3.5. Electron Energy Distribution Function

3.5.1. Initial electron energy distribution.* - The fission fragments ionize the He^3 and release electrons. For high-energy fragments whose velocity exceeds that of the orbital velocity of the electron, the binding energy of the electron can be neglected, and the collision regarded as Rutherford scattering. The differential cross section subtended is proportional to E_f^{-1}, where E_f is the energy of the fission fragment, and the electrons are expected to be in an initial energy distribution function, $f_1(\varepsilon) \propto \varepsilon^{-2}$, where ε is the energy of the electron. The maximum amount of energy handed over

* This description is based on discussions with J. Wilson of NASA/Langley Research Center.

to the electron is given by $\varepsilon_c \approx (2m/M)E_f$, where m is the electron mass, and M the mass of the fission fragment. The initial distribution function for electrons created by a fragment of energy $E_{f,1}$ is shown in figure 3.1 (solid curve). The picture fails around 1.5 ε_i, where ε_i is the ionization energy, or around 30 eV, as there are no more excitation levels, and the curve goes to a maximum and falls off at lower energies.

As the fission fragment slows down to an energy $E_{f,2}$, the cutoff drops to $\varepsilon_{c,2}$, and the distribution is now as shown by the dotted curve. The distribution function for all the electrons produced by one fission fragment is the sum of such curves, and will have a slope steeper than ε^{-2}.

3.5.2. Overall description of the average energy of one electron versus time. - Consider one electron created at a kinetic energy $\approx$ 1 keV. Its energy first decays rapidly by inelastic collisions with a characteristic time T_{in}, and by elastic collisions with a characteristic time $T_{e,n}$ (T_{in}, $T_{e,n} \propto v_r^{-1}$). In addition, cold electrons can cool the hot ones. Strong electron-electron cooling does not take place until the energies are low, as $\tau_{eq} \propto v_r^3$. However, at $\varepsilon \approx 1$ eV, $\tau_{eq,e\text{-}e} \approx T_{e,n}$, although there are 10^6 times more neutrals than electrons. The characteristic times for cooling are much less than the plasma containment time.

The electrons can gain energy from other electrons when at low energies by Coulomb collisions (section 3.2.4), and by collisions of the second kind with excited neutrals (superelastic collisions). However, the density of excited neutrals is probably of the order of the electron density and much less than that of unexcited neutrals, so collisions of the second kind are neglected.

The electrons, then, start off in a distribution as in figure 3.1, and then continuously lose energy until at low energies. For energies below 1 eV and $n \approx 10^{13}$, $\tau_{eq,e\text{-}e} << \tau_c$, the containment time, and therefore at low energies a Maxwellian distribution of electrons is attained, with a temperature approximately that of the neutral gas. Note that only electron-electron collisions ($\tau_{eq,e\text{-}e}$) lead to a Maxwellian distribution, while electron-neutral elastic collisions ($T_{e,n}$) need not. The latter reduce the electron energy; the former redistribute it. This model enables an estimate of the steady-state electron energy distribution to be made.

3.6. Simple Intuitive Description of the Steady-State Electron Energy Distribution Function

The intent of this section is to provide simple intuitive arguments to indicate the essential features of the electron energy distribution function and compare them with that of Hassan (ref. 6). The duration of a pulse is 5×10^{-4} s, and the lifetime of an electron $\approx 10^{-7}$ s; hence we assume there is a continuous constant source of electrons for the duration of the pulse. Each electron then starts at a high energy, loses energy with time, becomes Maxwellian at low energies, and is recombined.

The density, dn, of electrons in the energy interval ε to $\varepsilon + d\varepsilon$ is proportional to the amount of time, Δt, each electron spends in this interval,

$$dn \propto \Delta t$$

Now for one electron,

$$\lim_{\Delta\varepsilon \to 0} \frac{\Delta t}{\Delta \varepsilon} = \left(\frac{d\varepsilon}{dt}\right)^{-1}$$

where $\frac{d\varepsilon}{dt}$ is the rate of change of energy versus time for an average electron. Therefore,

$$dn = f(\varepsilon)d\varepsilon \propto \left(\frac{d\varepsilon}{dt}\right)^{-1} d\varepsilon$$

where $f(\varepsilon)$ is the steady-state electron energy distribution function, and

$$f(\varepsilon) \propto \left(\frac{d\varepsilon}{dt}\right)^{-1}$$

We now construct $f(\varepsilon)$ versus ε on a logarithmic plot (fig. 3.2). Starting from high energy, the region DE shows a sharp drop as ε increases, because the initial distribution of electrons is the sum of curves similar to figure 3.1; the exact shape of DE is not discussed further. Below about

35 eV, the electron energy loss is mainly from inelastic collisions, where $d\varepsilon/dt \propto \varepsilon^{1/2}$ from equation (4); hence in CD, $f(\varepsilon) \propto \varepsilon^{-1/2}$. The lower limit of the region C is around a volt (see section 2.2.2). Near C there is less and less contribution from excitation, and in BC electron-neutral collisions dominate. Here equation (8) indicates $d\varepsilon/dt \propto \varepsilon^{3/2}$, so $f(\varepsilon) \propto \varepsilon^{-3/2}$. Below B electron-electron collisions dominate, and as $\tau_{eq} << \tau_c$, a Maxwellian distribution is formed, with its peak at the temperature of the neutral gas at some hundreds of degrees Kelvin.

The values of the ordinate in figure 3.2 are not absolute, and an order of magnitude calculation enables a comparison to be made of the average density, n_{AB}, of electrons per unit energy in AB versus n_{CD} in CD. Assume AB extends over a range $\Delta\varepsilon_{AB} = 1$ eV, and CD over a range of $\Delta\varepsilon_{CD} = 30$ eV. Then,

$$\frac{N_{AB}}{t_{AB}} \Delta\varepsilon_{AB} \approx \frac{N_{CD}}{t_{CD}} \Delta\varepsilon_{CD}$$

where the times t_{AB}, t_{CD} correspond to those an average electron spends in AB and CD. Now $t_{AB} = \tau_c = 10^{-7}$ s, the recombination time, and $t_{CD} = T_{in} \simeq 0.4 \times 10^{-10}$ s. Therefore

$$\frac{n_{AB}}{n_{CD}} \approx 10^3 \text{ or } 10^4$$

The relative scale on the ordinate of figure 3.2 conforms with this ratio.

The essential details of figure 3.2 agree with an electron energy distribution curve of Hassan (ref. 6) derived from the Boltzmann equation (figure 3.3). Hassan actually plotted $f(\varepsilon)/\varepsilon^{1/2}$, and the curve for $f(\varepsilon)$ is due to Meador and Weaver (ref. 7). The points B and D in figure 3.2 occur in the same energy range as figure 3.3. Between B and D Hassan's curve shows $f(\varepsilon) \propto \varepsilon^{-1}$, whereas figure 3.2 shows $f(\varepsilon) \propto \varepsilon^{-1/2}$ near D, and $\propto \varepsilon^{-3/2}$ near B. Both curves show a Maxwellian distribution to the left of B with about 10,000 times more electrons in the Maxwellian distribution below 1 eV than there are in the non-Maxwellian distribution above it.

3.7. References

1. Wilson, J.: Private communication.

2. Biondi, M. A.; and Brown, S. C.: Phys. Rev., Vol. 75, p. 1700, 1949.

3. von Engel, A.: Ionized Gases. Oxford University Press, 2nd ed., 1955, fig. 27B, p. 47.

4. von Engel, A.: Ionized Gases, Oxford University Press, 2nd ed., 1955, p. 31.

5. Spitzer, L.: Physics of Fully Ionized Gases. Interscience Publishers, 2nd ed., 1962, ch. 5.

6. Hassan, H. A.; and Deese, J. E.: Phys. Fluids, Vol. 19, p. 2005, 1976.

7. Meador, W. M.; and Weaver, W. R.: Private communication.

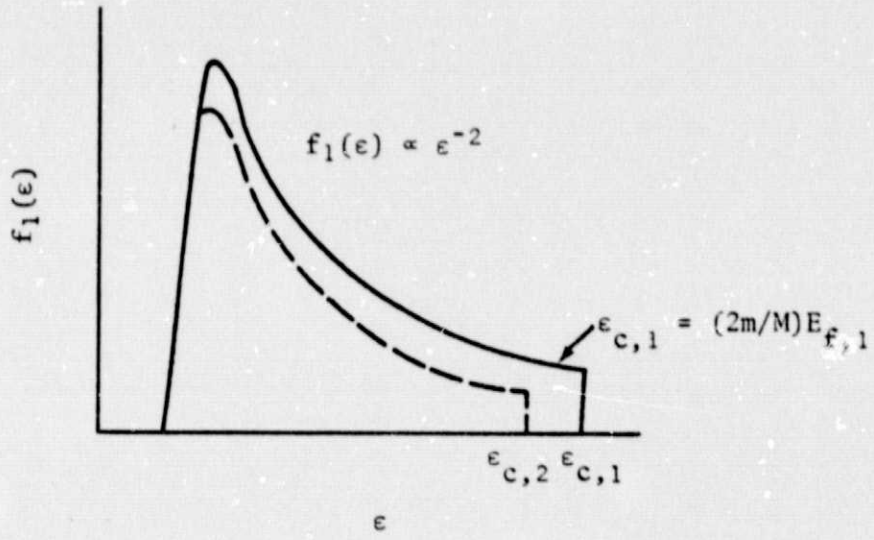

Figure 3.1. Initial distribution function $f_1(\varepsilon)$ for electrons; the curves are not normalized.

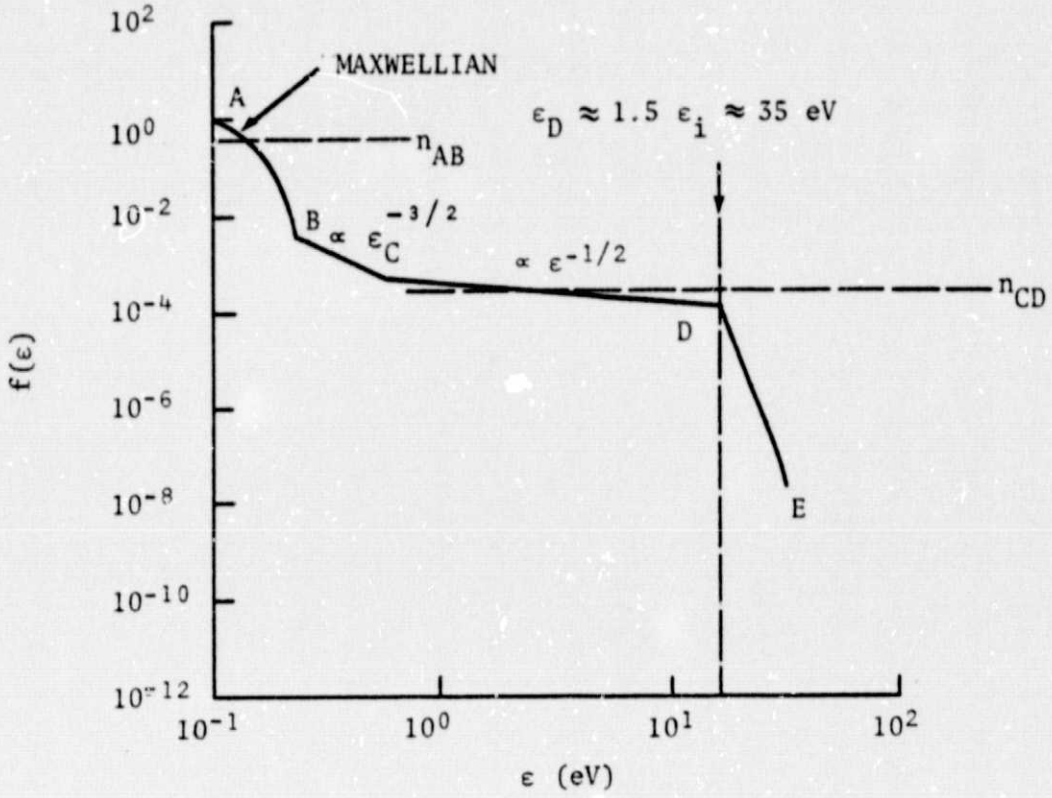

Figure 3.2. Steady-state electron energy distribution function.

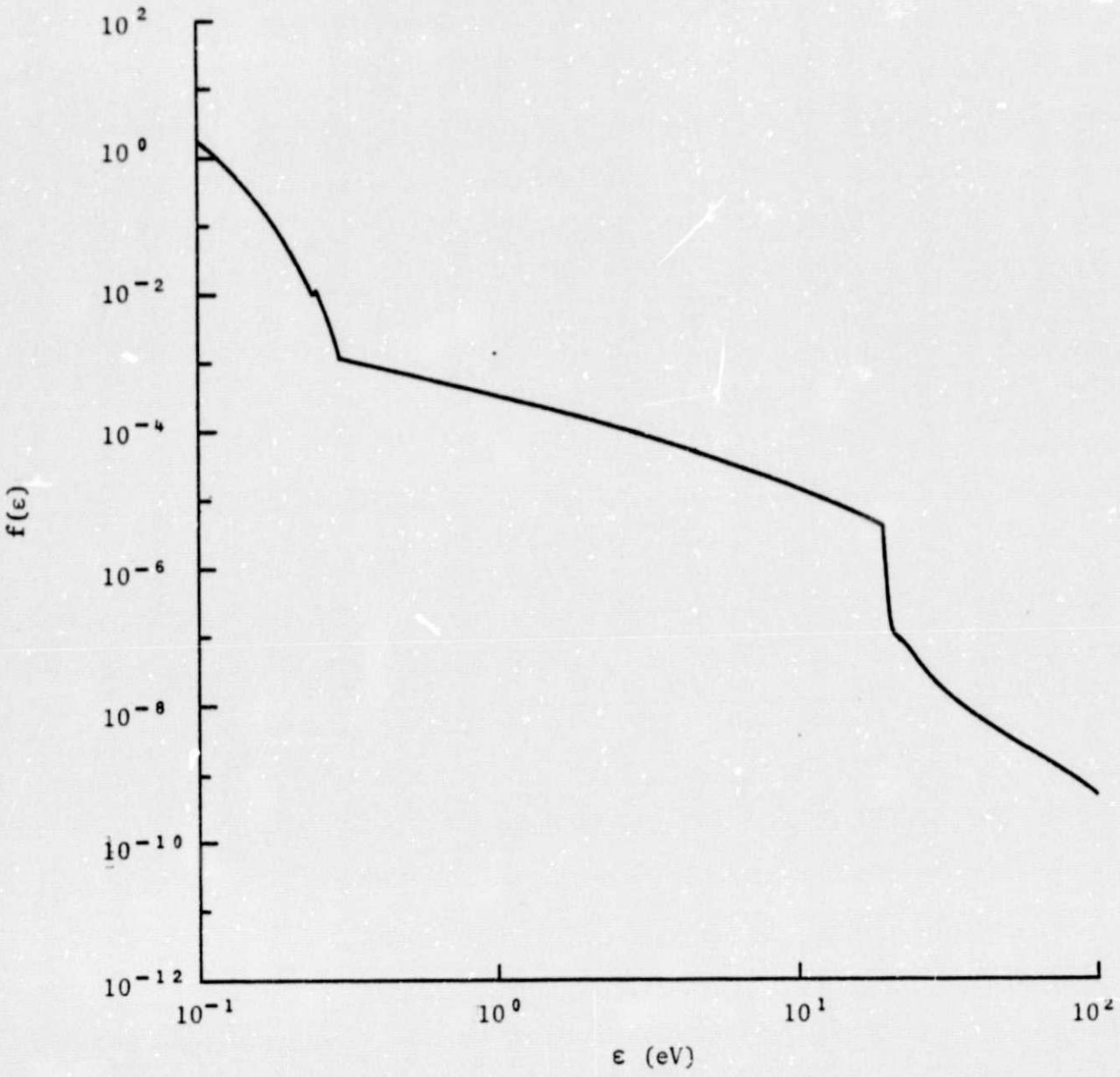

Figure 3.3. Electron energy distribution function $f(\varepsilon)$ after Hassan. (Flux 10^{16} cm^{-2}/s, p = 100 torr).

4. SIMPLIFIED MODEL OF A VOLUMETRIC DIRECT NUCLEAR-PUMPED ^{3}He-Ar LASER*

4.1. Introduction

Recently successful lasing was accomplished by the NASA/Langley Research Center team in a volumetric nuclear-pumped ^{3}He-Ar laser (refs. 1,2). It is the purpose of this paper to develop a simplified model for the laser, to establish which processes dominate and, in particular, to clarify the physics of the reactions.

The physical model (ref. 3) is described in section 2.2, and the source terms arising from the ^{3}He(n,p) ^{3}H reaction as well as the rate equations are given. Steady-state solutions are derived for the densities of the species versus the fraction of argon. The dominant pumping mechanism is collisional radiative recombination of the argon atomic ions, and subsequent radiative cascading into the upper laser level. The reactions following recombination are described in section 4.3, and an expression is derived for the difference in densities of the argon 3d and 4p levels (a quantity that should be nearly proportional to the output of the laser). Comparison with experiment indicates good agreement.

4.2. Physical Model

Neutrons from a reactor are thermalized and enter a vessel containing a ^{3}He-Ar mixture at a total pressure of order 1 atmosphere. The laser excitation energy is derived from the ^{3}He(n,p) ^{3}H reaction. The proton and triton possess 0.57 MeV and 0.19 MeV respectively, and excite and ionize the gases.

The major fraction of the energy released produces helium ions, He^+, and metastable atoms, He*. The He^+ is rapidly converted to He_2^+, which in turn is lost by charge transfer to neutral argon to form Ar^+. The He* is partially converted to He_2^*, and both He* and He_2^* ionize the argon by Penning

---

* Prepared by W. L. Harries of ODU and J. Wilson of NASA/LaRC and presented at the First International Symposium of Fission Induced Plasmas and Direct Nuclear Pumped Lasers, held at the Université Paris - Sud, Orsay, France, May 23-25, 1978.

ionization. Collisional-radiative recombination and argon molecular ion formation reduce the Ar^+ population. On recombination to neutral argon, the cascading excited atoms can form a population inversion between the 3d and 4p levels, which leads to lasing. It is of interest therefore to estimate the Ar^+ population density, especially as it relates to the recombination rate. The laser output depends on the Ar^+ recombination rate and various branching ratios for the processes occurring after recombination.

In estimating the Ar^+ density, rate equations for the various species were obtained (ref. 3). The species considered were He^+, He_2^+ (the He^+ converts rapidly to He_2^+, and both are lumped together as N^+), He^*, and He_2^* (lumped together as N^*), Ar^+, Ar_2^+, and the electron density; thus there are five coupled equations. The various reactions are given in tables 4.1 to 4.3, section 4.5, together with the values of the rate coefficients obtained from the literature. The rate coefficients are also labeled on figure 4.1. The densities of the various species depend on the relative argon concentration, which is described by the fraction c, where $0 < c < 1$.

The rate equations, with the various processes, labeled in figure 4.1 are

$$\frac{dN^+}{dt} = S^+(He) + xN^{*2} - (s + uN_o)N^+n - tn^2N^+ - (q + rN_o)N^+cN_o \qquad (1)$$

$$\frac{dN^*}{dt} = S^*(He) + (s + uN_o)N^+n + tN^+n^2 - 2xN^{*2} - yN^*n - pcN_oN^* \qquad (2)$$

$$\frac{dAr^+}{dt} = S^+(Ar) + pcN_oN^* + (q + rN_o)N^+cN_o - uN_oAr^+n - t'Ar^+n^2$$
$$- [v(1 - c) + wc]\, N_o^2cAr^+ \qquad (3)$$

$$\frac{dAr_2^+}{dt} = [v(1 - c) + wc]N_o^2cAr^+ - s_2Ar_2^+n \qquad (4)$$

$$n = N^+ + Ar^+ + Ar_2^+ \qquad (5)$$

Here the quantities naming the species correspond to the densities, and n is the electron density. Where more than one symbol is assigned a reaction in figure 4.1, the different rate coefficients correspond to different third bodies and are described later.

The source terms in the equations, S terms corresponding to the rate of production of excited and ionized species, are proportional to the rate of production of protons and tritons, and therefore proportional to F, the flux density of thermalized neutrons. The number of nuclear reactions per unit volume depends on the total gas pressure p and on d the tube diameter, since the neutron flux generally undergoes appreciable attenuation in crossing. With $p = 1$ atm, $d = 2$ cm, about 25 percent of the neutrons are absorbed in the gas (ref. 3), and therefore the source terms here are approximately proportional to Fp. The terms also depend on c, the Ar fraction, and with the above conditions are (ref. 3)

$$S^{+}(He) \approx 2 \times 10^{20} (1 - c)^2/(1 + 3c) \tag{6}$$

$$S^{*}(He) \approx 0.8 \times 10^{20} (1 - c)^2/(1 + 3c) \tag{7}$$

$$S^{+}(Ar) \approx 1.2 \times 10^{21} c(1 - c)/(1 + 3c) \tag{8}$$

Although computer graphical solutions of the densities were readily obtainable for the steady state, they did not clearly indicate which processes dominated. Therefore, approximate analytical solutions were attempted. The method was to use the computer solutions for comparison and to neglect small terms. The computer sclutions showed that n, the electron density, was almost independent of c as long as c did not approach unity. It might be expected that this would be roughly so, because the energy level schemes of He and Ar are fairly similar and the recombination times of the different ion species are approximately the same at equal ion densities. Thus a trial value of n independent of c was assumed.

The magnitudes of the various terms were compared for a neutral density $N_o = 3 \times 10^{19}$ cm^{-3} and (from exact computer solutions) $n = 10^{13}$ cm^{-3} and $4 \times 10^{12} < N^* < 10^{14}$. It has been found experimentally that lasing ceases if c is more than 0.2, so c was assumed between 0 and 0.1 when comparing terms.

The recombination terms s, u, t, can be neglected in equation (2), as well as superelastic collisions, y. In the steady state the equation then reduces to a quadratic, but it is convenient to give solutions in two regimes depending on c:

$$N^* = \begin{cases} [S^*(He)/2x]^{1/2} ; & c < 10^{-4} \quad (9a) \\ S^*(He)/pcN_o ; & c > 10^{-4} \quad (9b) \end{cases}$$

The dominant source term S^* corresponds to electrons exciting neutral helium atoms. When there is little argon present, the source term is balanced by losses of He^* to He_2^+ [eq. (9a)]. When there is appreciable argon present the losses of He^* and He_2^* are by Penning ionization of argon [eq. (9b)]. The quantity pcN_o has the dimensions time^{-1}, so we define a characteristic time for the loss of He^* and He_2^* by Penning ionization:

$$\tau^* = (pcN_o)^{-1} \quad (10)$$

Hence equation (9b), which applies to the range of experimental interest, can also be expressed as:

$$N^* = S^*(He)\tau^* ; \quad c > 10^{-4} \quad (11)$$

The formation of He_2^+ from He^+ is a rapid process, and the quantity N^+, the sum of the two densities, is essentially the density of He_2^+. The solution of N^+ from equation (1) depends on whether c is less than or greater than 10^{-4}. If $c < 10^{-4}$, the charge transfer terms (q,r) can be neglected. The dissociative recombination term s, and the recombination with He as a third body, u, are also small. Assuming $n = N^+$, then as N^* is known, equation (1) becomes a cubic in N^+.

On the other hand, if $c >> 10^{-4}$, the charge transfer terms are now important. Again the recombination of He_2^+ to He^* (s, t, u) can be neglected. The solutions in the different regimes of c are

$$N^+ = \begin{cases} \left[\dfrac{S^+(He) + S^*(He)/2}{t}\right]^{1/3} ; & c < 10^{-4} \quad (12a) \\ \dfrac{S^+(He) + x\left(S^*(He)/pcN_o\right)}{(q + rN_o)cN_o} \simeq \dfrac{S^+(He)}{(q + rN_o)cN_o} ; & c > 10^{-4} \quad (12b) \end{cases}$$

The N^+ is formed by direct electron ionization of He and by the formation of He_2^+ from the He* + He* reaction. When there is little argon present, the He_2^+ is lost by recombination, (t term), where the dominating process is $He_2^+ + 2e \rightarrow He^* + He + e$. With appreciable argon present, the formation of He_2^+ from He* + He* is unimportant as the He* is depleted by Penning ionization of argon. The loss of He_2^+ is now mainly by charge transfer to argon (q and r).

The quantity $(q + rN_o)cN_o$ has the dimensions of time^{-1}, so equation (12b) can be rewritten

$$N^+ = S^+(He)\tau^+ \quad ; \quad c > 10^{-4} \quad (12c)$$

where $\tau^+ = [(q + rN_o)cN_0]^{-1}$ is a characteristic loss time for He_2^+ by charge transfer.

Equation (3) gives two solutions for Ar^+ depending on whether $c >> 10^{-4}$ or not. It is convenient to consider large c first. None of the terms can now be neglected, and

$$Ar^+ = \frac{S^+(He) + S^*(He) + S^+(Ar)}{[v(1 - c) + wc]N_o^2c + [u'N_on + t'n^2]} ; \quad c >> 10^{-4} \quad (13)$$

where the terms in the numerator are obtained from equations (9b) and (12b). The production of Ar^+ is due to direct ionization through $S^+(Ar)$, to Penning ionization which depends on S*(He), and also to charge transfer, which depends on $S^+(He)$. The sum of the three terms can be defined as a total source term S. The denominator represents the loss processes: the first parenthesis

corresponds to the loss of Ar^+ into Ar_2^+ (v, w terms), the second due to Ar^+ recombining (u', t'). Characteristic loss times for these processes may be defined:

$$\tau_2 = \left[\left(v(1 - c) + wc\right) N_o^2 c\right]^{-1} \tag{14}$$

$$\tau_3 = [u'N_o n + t'n^2]^{-1} \tag{15}$$

and if both processes occur simultaneously, the overall loss time τ_1 is given by

$$\tau_1^{-1} = \tau_2^{-1} + \tau_3^{-1} \tag{16}$$

Equation (13) can also be expressed as

$$Ar^+ = S\tau_1 \quad ; \quad c >> 10^{-4} \tag{17}$$

If $c < 10^{-4}$, the v and w terms corresponding to the formation of Ar^+ can be neglected, and from equation (3)

$$Ar^+ = \frac{S^+(Ar) + pcN_oN^* + (q + rN_o)N^+cN_o}{u'N_o n + t'n^2} \quad ; \quad c < 10^{-4} \tag{18}$$

The numerator is the sum of three source terms as before. However, the values of N^* and N^+ are those corresponding to $c < 10^{-4}$ or given by equations (9a) and (12a). The three source terms may be added to give a total source term S_o, corresponding to small c. In addition, now $n \to N^+$. The denominator represents loss of Ar^+ by recombination, so

$$Ar^+ = S_o\tau_3 \quad ; \quad c < 10^{-4} \tag{19}$$

Over the range of c:

$$Ar^+ = \begin{cases} S_o\tau_3 \quad ; \quad c < 10^{-4} & \text{(20a)} \\ S\tau_1 \quad ; \quad c >> 10^{-4} & \text{(20b)} \end{cases}$$

The density of Ar^+ is now immediately obtained from equation (4). When c is small the Ar_2^+ density is much smaller than for the other species. Otherwise:

$$Ar_2^+ = \frac{S}{s_2 n \left[1 + \frac{u' N_o n + t' n^2}{\left(v(1 - c) + wc\right) N_o^2 c}\right]} \quad ; \quad c >> 10^{-4} \tag{21}$$

The $s_2 n$ corresponds to loss of Ar_2^+ by recombination to Ar*, and into the 4p level, so if a characteristic loss time is defined

$$\tau_4 = (s_2 n)^{-1} \tag{22}$$

then equation (21) becomes

$$Ar_2^+ = S\tau_4\left(\frac{\tau_3}{\tau_2 + \tau_3}\right) \tag{23}$$

The quantity $\tau_3/(\tau_2 + \tau_3)$ is the branching ratio, or the fraction of Ar^+ that recombines through the Ar' channel in figure 4.1. A comparison of the simplified expressions for the densities versus c (dotted) with exact computer solutions including all the terms (fig. 4.2) shows good agreement within a factor of two.

4.3. Conditions After Recombination

Laser action results when the upper neutral Argon 3d level population exceeds the 4p level. After recombination, the 3d level is fed by the Ar neutrals cascading down in energy from the Saha region, Ar' in figure 4.3. Some of the atoms may not reach the 3d level because of collisional deexcitation, and/or spontaneous emission of quanta to energies below the 3d level. Also, the energy levels in the Ar' region exceed those for the formation of Ar_2^+, and there is the possibility of the reaction $Ar' + Ar \rightarrow Ar_2^+ + e$, the Hornbeck-Molnar effect. We have included the effect of collisional deexcitation, spontaneous emission, and the Hornbeck-Molnar effect by describing them with

characteristic times and including them in our calculations. The resulting gain does not agree with the observed laser output if these effects are significant, we believe that these effects (shown dotted in fig. 4.3) are unimportant.

The Ar^+ can also be lost by formation of Ar_2^+ (fig. 4.3) with the characteristic time τ_2. The Ar_2^+ can dissociatively recombine to give a neutral argon in the 4p level, which should reduce the laser output (ref. 4). We have investigated the possibility that a fraction of the Ar_2^+ density fills levels other than the 4p, i.e., either the 3d level or levels below the 4p, and again find disagreement with experiment. Thus the flow paths that dominate are those shown by solid lines. Then the difference in densities of the 3d and 4p levels can be estimated in terms of the times τ_2, τ_3 and the lifetimes τ_{3d}, τ_{4p} of the levels.. The difference in densities should be proportional to the gain G of the laser, and

$$G \propto Ar^+ \left[\tau_{3d}\tau_3^{-1} - \tau_{4p}(\tau_2^{-1} + \tau_3^{-1})\right] \tag{24}$$

$$\propto S\left[\tau_{3d}\left(\frac{\tau_2}{\tau_2 + \tau_3}\right) - \tau_{4p}\right] \tag{25}$$

4.4. Comparison with Experiment

Figure 4.4 shows G and Ar^+ plotted versus c and compared with the experimental results (refs. 1, 2). Error bars are not shown, but the experimental results are within ±30 percent. The ordinate values are not absolute, and G was normalized to the experimental results. The experimental cutoff at $c \approx 0.2$ due to dissociative recombination of Ar_2^+ into the 4p level occurs when there is still ample density of Ar^+, and seems consistent with the value of G.

In summary, for low values of c the output increases with the fraction of argon, but if c is made too high, laser action is curtailed by the formation of Ar_2^+ which dissociatively recombines to fill the 4p level.

4.5. Helium/Argon Rate Coefficients

Table 4.1. Helium rate coefficients.

Reaction	Symbol	Rate Coefficient	Reference
$He_2^+ + e \rightarrow He^* + He$	s	1×10^{-8}	5
$He_2^+ + 2e \rightarrow He^* + He + e$	t	$(4 \pm 0.5) \times 10^{-20}$	6
$He_2^+ + e + He \rightarrow He^* + 2He$	u	$(5 \pm 1) \times 10^{-27}$	6
$He^* + He^* \rightarrow He_2^+ + e$	x	$(1.5 \pm 0.3) \times 10^{-9}$	6
$He^* + e \rightarrow He + e$	y	$(4.2 \pm 0.6) \times 10^{-9}$	6

Table 4.2. Argon rate coefficients.

Reaction	Symbol	Rate Coefficient	Reference
$Ar^+ + 2e \rightarrow Ar^* + e$	t'	$\sim 9 \times 10^{-20}$	7
$Ar^+ + e + Ar \rightarrow Ar^* + Ar$	u'	$\sim 1 \times 10^{-26}$	7
$Ar^+ + 2Ar \rightarrow Ar_2^+ + Ar$	w	$\left(2.5\ {}^{+1.9}_{-1.0}\right) \times 10^{-31}$	8
$Ar_2^+ + e \rightarrow Ar^* + Ar$	s_2	$(7 \pm 1) \times 10^{-7}$	9

Table 4.3. Helium-argon rate coefficients.

Reaction	Symbol	Rate Coefficient	Reference
$He_2^+ + e + Ar \rightarrow He^* + He + Ar$	$\sim$u	$\sim 5 \times 10^{-27}$	----
$He_2^* + Ar \rightarrow Ar^+ + He + e$	p	$(7 \pm 1) \times 10^{-11}$	10
$He_2^+ + Ar \rightarrow Ar^+ + 2He$	q	2.2×10^{-10}	11
$He_2^+ + Ar + He \rightarrow Ar^+ + 3He$	r	$(24 \pm 6) \times 10^{-30}$	11
$Ar^+ + Ar + He \rightarrow Ar_2^+ + He$	v	$\sim 1 \times 10^{-31}$	8
$Ar^+ + e + He \rightarrow Ar^* + He$	$\sim$u'	$\sim 1 \times 10^{-26}$	----

4.6. References

1. Jalufka, N. W.; DeYoung, R. J.; Hohl, F.; and Williams, M. D.: Appl. Phys. Lett., Vol. 29, p. 188, 1976.

2. DeYoung, R. J.; Jalufka, N. W.; Hohl, F.; and Williams, M. D.: Direct Nuclear Pumped Lasers Using the Volumetric ^{3}He Reaction. The Princeton University Conference on Partially Ionized and Uranium Plasmas, p. 96, Sept. 1976.

3. Wilson, J. W.; DeYoung, R. J.; and Harries, W. L.: Nuclear Pumped ^{3}He-Ar Laser Modeling. Submitted to J. Appl. Phys.

4. Lorents, D. C.: Physica, Vol. 82C, p. 19, 1976.

5. Johnson, A. W.; and Gerado, J. B.: Phys. Rev., Vol. A5, p. 1410, 1972.

6. Deloche, R.; Monchicourt, P.; Cheret, M.; and Lambert, F.: Phys. Rev., Vol. A13, p. 1140, 1976.

7. Hinnov, E.; and Hirschberg, J. G.: Phys. Rev., Vol. 125, p. 795, 1962.

8. McDaniel, E. W.; Cermak, V.; Dalgarno, A.; Ferguson, E. E.; and Friedman, L.: Ion Molecule Reactions, Wiley Interscience, 1970.

9. Biondi, M. A.: Phys. Rev., Vol. 129, p. 1181, 1963.

10. Schmeltekopf, A. L.; and Fehsenfeld, F. C.: J. Chem. Phys., Vol. 53, p. 3173, 1970.

11. Lee, F. W.; Collins, C. B.; and Waller, R. A.: J. Chem. Phys., Vol. 65, p. 1605, 1976.

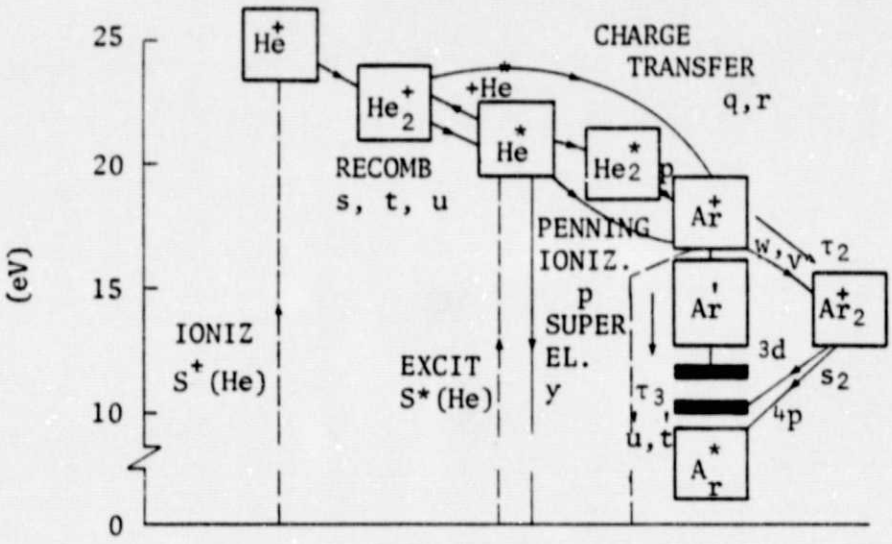

Figure 4.1. Flow chart of processes in the ^{3}He-Ar Laser. (Dashed lines show source terms).

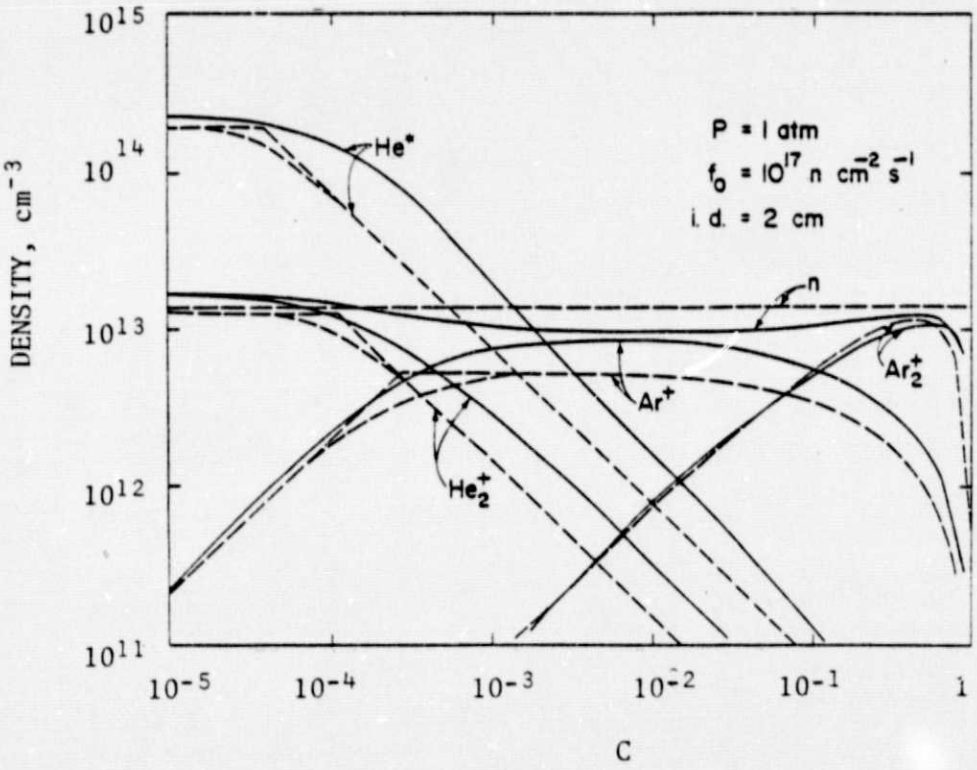

Figure 4.2. Comparison of approximate analytical solutions for the densities (dashed) and exact computer solutions (continuous lines).

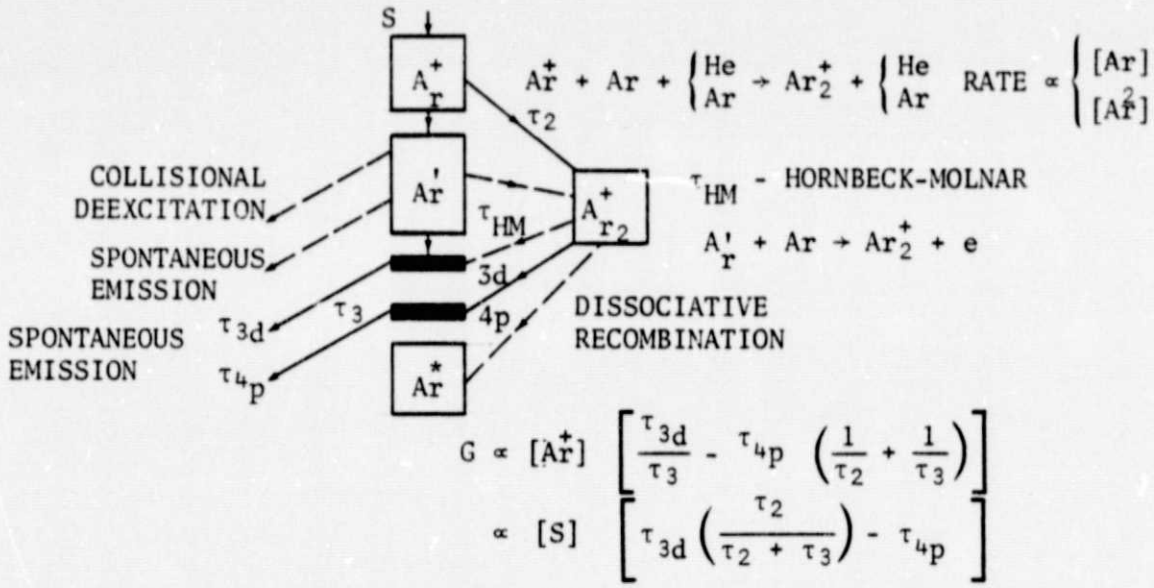

Figure 4.3. Processes occurring after recombination. The processes shown with dashed lines are unimportant.

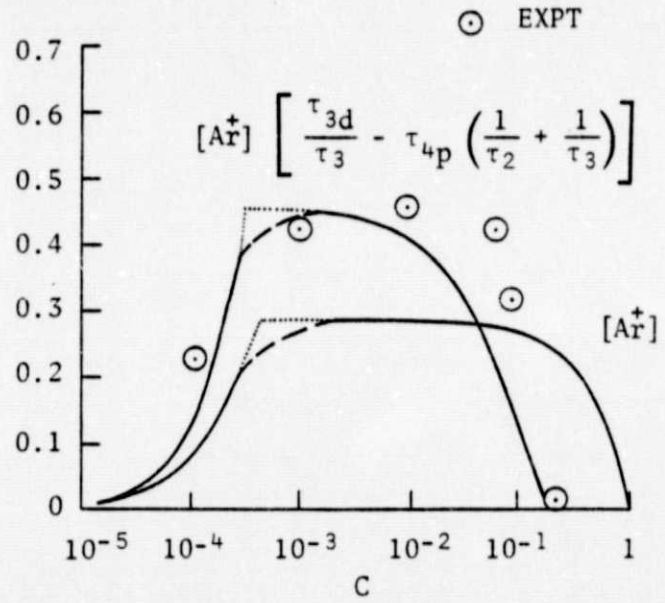

Figure 4.4. Comparison with experiment.

5. LIST OF PUBLICATIONS AND TALKS RESULTING FROM GRANT NSG 1362

Reports

"Fission Induced Plasmas." W. L. Harries, Progress Report for July 1, 1977 to Dec. 31, 1977. Technical Report - PGSTR-PH78-2.

"Fission Induced Plasmas." W. L. Harries and Yuehjaw J. Shiu, Progress Report for Jan. 1, 1978 to June 30, 1978. Technical Report PTR-78-11.

Papers Presented at Professional Meetings

"Simplied Model of a Volumetric Direct Nuclear-Pumped ^{3}He-Ar Laser." W. L. Harries and J. W. Wilson, First International Symposium on Fission Induced Plasma and Nuclear Pumped Lasers, Université de Paris, Centre D'Orsay, 23-25 May 1978.

"Plasma Properties in Connection with Gas Lasers." J. W. Wilson, W. L. Harries and R. J. DeYoung, Virginia Academy of Science, Blacksburg, Virginia, 9-13 May 1978.

Papers

"Mechanisms of the ^{3}He-Ar Direct Nuclear-Pumped Laser." J. W. Wilson, R. J. DeYoung and W. L. Harries, J. Appl. Phys. (Jan. 1979, in press).

"Simplified Model of a Volumetric Direct Nuclear-Pumped ^{3}He-Ar Laser." W. L. Harries and J. W. Wilson, Proceedings of the First International Symposium on Fission Induced Plasmas and Nuclear Pumped Lasers, Université de Paris, Centre D'Orsay, 23-25 May 1978.